Belle Preprint *2009-23*
KEK Preprint *2009-26*



# Measurement of the branching fractions and the invariant mass distributions for $\tau^- \to h^- h^+ h^- \nu_\tau$ decays

M. J. Lee,[34] H. Aihara,[42] K. Arinstein,[1,30] V. Aulchenko,[1,30] T. Aushev,[16,11] A. M. Bakich,[37] E. Barberio,[20] A. Bay,[16] K. Belous,[10] V. Bhardwaj,[32] M. Bischofberger,[22] A. Bondar,[1,30] A. Bozek,[26] M. Bračko,[18,12] T. E. Browder,[6] P. Chang,[25] A. Chen,[23] P. Chen,[25] B. G. Cheon,[5] I.-S. Cho,[46] Y. Choi,[36] J. Dalseno,[19,39] A. Das,[38] W. Dungel,[9] S. Eidelman,[1,30] D. Epifanov,[1,30] M. Fujikawa,[22] N. Gabyshev,[1,30] A. Garmash,[1,30] H. Ha,[14] J. Haba,[7] B.-Y. Han,[14] Y. Hasegawa,[35] K. Hayasaka,[21] H. Hayashii,[22] Y. Hoshi,[41] W.-S. Hou,[25] Y. B. Hsiung,[25] H. J. Hyun,[15] T. Iijima,[21] K. Inami,[21] R. Itoh,[7] M. Iwasaki,[42] Y. Iwasaki,[7] T. Julius,[20] D. H. Kah,[15] J. H. Kang,[46] N. Katayama,[7] T. Kawasaki,[28] C. Kiesling,[19] H. J. Kim,[15] H. O. Kim,[15] J. H. Kim,[36] S. K. Kim,[34] Y. I. Kim,[15] Y. J. Kim,[4] B. R. Ko,[14] S. Korpar,[18,12] P. Križan,[17,12] P. Krokovny,[7] T. Kumita,[43] A. Kuzmin,[1,30] Y.-J. Kwon,[46] S.-H. Kyeong,[46] J. S. Lange,[3] S.-H. Lee,[14] J. Li,[6] C. Liu,[33] Y. Liu,[21] D. Liventsev,[11] R. Louvot,[16] J. MacNaughton,[7] F. Mandl,[9] S. McOnie,[37] H. Miyata,[28] Y. Miyazaki,[21] T. Mori,[21] E. Nakano,[31] M. Nakao,[7] H. Nakazawa,[23] Z. Natkaniec,[26] S. Nishida,[7] O. Nitoh,[44] S. Ogawa,[40] T. Ohshima,[21] S. Okuno,[13] S. L. Olsen,[34,6] P. Pakhlov,[11] G. Pakhlova,[11] H. Palka,[26] C. W. Park,[36] H. Park,[15] H. K. Park,[15] L. S. Peak,[37] R. Pestotnik,[12] M. Petrič,[12] L. E. Piilonen,[45] A. Poluektov,[1,30] S. Ryu,[34] H. Sahoo,[6] K. Sakai,[28] Y. Sakai,[7] O. Schneider,[16] A. J. Schwartz,[2] K. Senyo,[21] M. E. Sevior,[20] M. Shapkin,[10] V. Shebalin,[1,30] C. P. Shen,[6] J.-G. Shiu,[25] B. Shwartz,[1,30] J. B. Singh,[32] P. Smerkol,[12] A. Sokolov,[10] E. Solovieva,[11] S. Stanič,[29] M. Starič,[12] T. Sumiyoshi,[43] G. N. Taylor,[20] Y. Teramoto,[31] I. Tikhomirov,[11] S. Uehara,[7] K. Ueno,[25] Y. Unno,[5] S. Uno,[7] P. Urquijo,[20] Y. Ushiroda,[7] Y. Usov,[1,30] G. Varner,[6] K. Vervink,[16] A. Vinokurova,[1,30] C. H. Wang,[24] P. Wang,[8] Y. Watanabe,[13] R. Wedd,[20] E. Won,[14] B. D. Yabsley,[37] Y. Yamashita,[27] M. Yamauchi,[7] C. Z. Yuan,[8] C. C. Zhang,[8]

Z. P. Zhang,[33] V. Zhilich,[1,30] V. Zhulanov,[1,30] T. Zivko,[12] A. Zupanc,[12] and O. Zyukova[1,30]

(The Belle Collaboration)

[1]*Budker Institute of Nuclear Physics, Novosibirsk*

[2]*University of Cincinnati, Cincinnati, Ohio 45221*

[3]*Justus-Liebig-Universität Gießen, Gießen*

[4]*The Graduate University for Advanced Studies, Hayama*

[5]*Hanyang University, Seoul*

[6]*University of Hawaii, Honolulu, Hawaii 96822*

[7]*High Energy Accelerator Research Organization (KEK), Tsukuba*

[8]*Institute of High Energy Physics, Chinese Academy of Sciences, Beijing*

[9]*Institute of High Energy Physics, Vienna*

[10]*Institute of High Energy Physics, Protvino*

[11]*Institute for Theoretical and Experimental Physics, Moscow*

[12]*J. Stefan Institute, Ljubljana*

[13]*Kanagawa University, Yokohama*

[14]*Korea University, Seoul*

[15]*Kyungpook National University, Taegu*

[16]*École Polytechnique Fédérale de Lausanne (EPFL), Lausanne*

[17]*Faculty of Mathematics and Physics, University of Ljubljana, Ljubljana*

[18]*University of Maribor, Maribor*

[19]*Max-Planck-Institut für Physik, München*

[20]*University of Melbourne, School of Physics, Victoria 3010*

[21]*Nagoya University, Nagoya*

[22]*Nara Women's University, Nara*

[23]*National Central University, Chung-li*

[24]*National United University, Miao Li*

[25]*Department of Physics, National Taiwan University, Taipei*

[26]*H. Niewodniczanski Institute of Nuclear Physics, Krakow*

[27]*Nippon Dental University, Niigata*

[28]*Niigata University, Niigata*

[29]*University of Nova Gorica, Nova Gorica*

[30]*Novosibirsk State University, Novosibirsk*

[31]*Osaka City University, Osaka*

[32]*Panjab University, Chandigarh*

[33]*University of Science and Technology of China, Hefei*

[34]*Seoul National University, Seoul*

[35]*Shinshu University, Nagano*

[36]*Sungkyunkwan University, Suwon*

[37]*School of Physics, University of Sydney, NSW 2006*

[38]*Tata Institute of Fundamental Research, Mumbai*

[39]*Excellence Cluster Universe, Technische Universität München, Garching*

[40]*Toho University, Funabashi*

[41]*Tohoku Gakuin University, Tagajo*

[42]*Department of Physics, University of Tokyo, Tokyo*

[43]*Tokyo Metropolitan University, Tokyo*

[44]*Tokyo University of Agriculture and Technology, Tokyo*

[45]*IPNAS, Virginia Polytechnic Institute and State University, Blacksburg, Virginia 24061*

[46]*Yonsei University, Seoul*

## Abstract

We present a study of $\tau^- \to \pi^-\pi^+\pi^-\nu_\tau$, $\tau^- \to K^-\pi^+\pi^-\nu_\tau$, $\tau^- \to K^-K^+\pi^-\nu_\tau$, and $\tau^- \to K^-K^+K^-\nu_\tau$ decays using a 666 fb$^{-1}$ data sample collected with the Belle detector at the KEKB asymmetric-energy $e^+e^-$ collider at and near a center-of-mass energy of 10.58 GeV. The branching fractions are measured to be: $\mathcal{B}(\tau^- \to \pi^-\pi^+\pi^-\nu_\tau) = (8.42 \pm 0.00^{+0.26}_{-0.25}) \times 10^{-2}$, $\mathcal{B}(\tau^- \to K^-\pi^+\pi^-\nu_\tau) = (3.30 \pm 0.01^{+0.16}_{-0.17}) \times 10^{-3}$, $\mathcal{B}(\tau^- \to K^-K^+\pi^-\nu_\tau) = (1.55 \pm 0.01^{+0.06}_{-0.05}) \times 10^{-3}$, and $\mathcal{B}(\tau^- \to K^-K^+K^-\nu_\tau) = (3.29 \pm 0.17^{+0.19}_{-0.20}) \times 10^{-5}$, where the first uncertainty is statistical and the second is systematic. These branching fractions do not include contributions from modes in which a $\pi^+\pi^-$ pair originates from a $K^0_S$ decay. We also present the unfolded invariant mass distributions for these decays.

PACS numbers: 13.35.Dx, 12.15.Hh, 14.60.Fg

## INTRODUCTION

The decays of the $\tau$ lepton into three pseudoscalar particles can provide information on hadronic form factors, $K^*$ resonance spectroscopy, and the Wess-Zumino anomaly [1], and also can be used for studies of CP violation in the leptonic sector [2]. By studying decays into final states that contain one or three kaons, it is possible to extract strange spectral functions, which can be used for a direct determination of the strange quark mass and the Cabibbo-Kobayashi-Maskawa (CKM) matrix element $|V_{us}|$ [3–5]. These three hadron decays have been studied since the initial discovery of the $\tau$ lepton, but only the decay to three charged pions has been closely investigated. Even for this mode, measurements of its branching fraction have only been provided by the CLEO [6] and BaBar [7] groups. For all other modes, there are still many unresolved problems. For example, the branching fraction for $\tau^- \to K^-\pi^+\pi^-\nu_\tau$ decay recently measured by the BaBar collaboration [7] is significantly lower than the values from most previous measurements [8]; there is large scatter in the measured central values, which is reflected in the large scale factor (2.1) applied by the Particle Data Group when forming their average [8]. Intermediate two- and three-body resonance states in this decay have been previously studied but only with limited statistical precision, see, e.g., Refs [9–11]. There is evidence for quite rich dynamics, with strong signals for the $K_1(1270)$, $K_1(1400)$ and $K^*(1410)$ resonances in the three-body final state; other resonances can be seen in various two-body sub-systems. Theoretically, two intermediate resonances, the $\rho(770)^0$ and $K^*(892)^0$ (or its excitations), are expected to contribute to $\tau$ decay into $K^-\pi^+\pi^-\nu_\tau$: $\tau^- \to K^-\rho(770)^0(\to \pi^+\pi^-)\nu_\tau$ and $\tau^- \to K^*(892)^0(\to K^-\pi^+)\pi^-\nu_\tau$ [12]. These are shown in Figs 1(a) and (b), respectively.

Here we present new measurements of the branching fractions for $\tau^- \to \pi^-\pi^+\pi^-\nu_\tau$, $\tau^- \to K^-\pi^+\pi^-\nu_\tau$, $\tau^- \to K^-K^+\pi^-\nu_\tau$, and $\tau^- \to K^-K^+K^-\nu_\tau$ decays. (Unless otherwise specified, the charge-conjugate decay is also implied throughout this paper.) Events in which a $\pi^+\pi^-$ pair is consistent with a $K^0_S$ decay are excluded. Because of particle misidentification, measurements of all four of the above modes are correlated and, thus, are considered simultaneously.

We use a data sample of 666 fb$^{-1}$ collected with the Belle detector at the KEKB asymmetric-energy $e^+e^-$ collider [13] on the $\Upsilon(4S)$ resonance, 10.58 GeV, and 60 MeV below it (off-resonance). This sample contains $6.12 \times 10^8$ produced $\tau$-pairs. The Belle de-

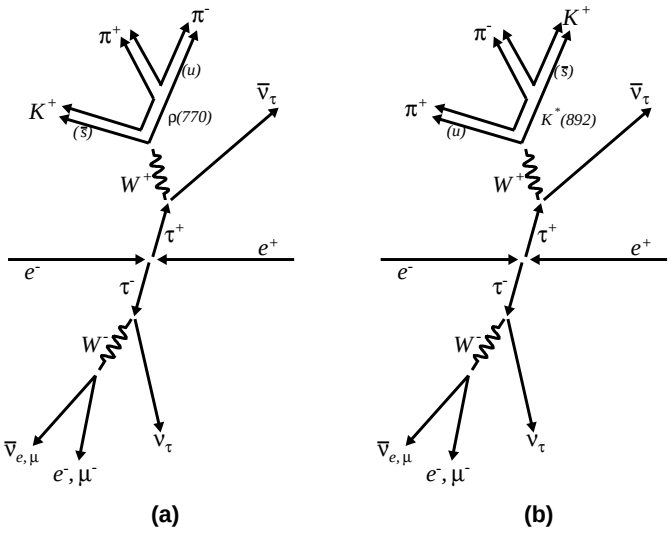


FIG. 1: A schematic view of $e^+e^- \to \tau^+\tau^-$ in the center-of-mass system, where one $\tau$ ($\tau^+$) decays to the signal mode ($\tau^+ \to K^+\pi^-\pi^+\nu_\tau$) and the other $\tau$ ($\tau^-$) decays to a leptonic mode ($\tau^- \to e^-\nu_\tau\overline{\nu}_e$ or $\tau^- \to \mu^-\nu_\tau\overline{\nu}_\mu$). Each figure shows one of two possible intermediate resonant states in the signal mode.

tector is a large-solid-angle magnetic spectrometer that consists of a silicon vertex detector (SVD), a 50-layer central drift chamber (CDC), an array of aerogel threshold Cherenkov counters (ACC), a barrel-like arrangement of time-of-flight scintillation counters (TOF), and an electromagnetic calorimeter (ECL) comprised of CsI(Tl) crystals located inside a superconducting solenoid coil that provides a 1.5 T magnetic field. An iron flux return located outside the coil (KLM) is instrumented to detect $K_L^0$ mesons and to identify muons. The detector is described in detail elsewhere [14].

## SELECTION OF EVENTS

Three-prong decays of the $\tau$ are selected from candidate $\tau^+\tau^-$ pair events as follows. We use events where the number of charged tracks is four and the sum of their charges is zero; the transverse momentum of each track in the laboratory frame is required to be larger than 0.1 GeV/$c$, and the tracks should extrapolate back to the interaction point within $\pm$5 cm along the beam direction and $\pm$1 cm in the transverse plane. The sum of the reconstructed

momenta in the center-of-mass (CM) frame is required to be less than 10 GeV/$c$, and the sum of energies deposited in the calorimeter is required to be less than 10 GeV. The largest of the four tracks' transverse momenta is required to be greater than 0.5 GeV/$c$ to reject two-photon events, which typically have low transverse momentum tracks. To reject beam-related background, we require the position of the reconstructed event vertex to be less than 3 cm from the interaction point along the beam direction, and separated by less than 0.5 cm in the transverse plane. The missing mass, $M^2_{\rm miss} = (p_{\rm init} - \sum_{\rm tr} p_{\rm tr} - \sum_\gamma p_\gamma)^2$, and the polar angle of the missing momentum in the CM frame are efficient variables for rejecting two-photon and Bhabha backgrounds. In the definition of the missing mass, $p_{\rm tr}$ and $p_\gamma$ are the four-momenta of measured tracks and photons, respectively, and $p_{\rm init}$ is the initial CM frame four-momentum of the $e^+e^-$ beams. We require that the missing mass be larger than 1 GeV/$c^2$ and less than 7 GeV/$c^2$, and that the polar angle with respect to the beam direction in the CM frame be larger than 30° and less than 150°. Detailed information on the $\tau^+\tau^-$ pair selection and background suppression using missing mass can be found in [15].

Particle identification is used to select $\tau$ events that contain one lepton (electron or muon) and three hadrons (pions or kaons). The magnitude of thrust is evaluated and is required to be larger than 0.9 to suppress two-photon and $e^+e^- \to q\bar{q}$ backgrounds, where the thrust is defined by the maximum of $(\sum_i |\hat{n} \cdot \vec{p_i}|)/(\sum_i |\vec{p_i}|)$. Here $\vec{p_i}$ is the momentum of the $i$-th track and $\hat{n}$ is the unit vector in the direction of the thrust axis – the direction maximizing the thrust. We require that the angle between the total momentum of the hadrons and the lepton momentum in the CM system be larger than 90°, since the tag-side lepton and signal-side hadrons usually lie in opposite hemispheres: the so-called 1–3 prong configuration, due to the large transverse momenta of $\tau$ leptons. The invariant mass of charged tracks and gamma clusters on each side is required to be less than the $\tau$ mass. Finally, we require that there be no $K^0_S$, $\pi^0$, or energetic $\gamma$ on the signal side, where the selection criteria for these particles are described below. Figure 2 shows distributions of the variables used to select the 1–3 prong sample, where in each case, the selection value is indicated by a vertical line in the figure. The surviving events are candidates for $\tau^- \to h_1^- h_2^+ h_3^- \nu_\tau$, where $h_{1,2,3}$ is either a pion or a kaon candidate. At this stage, the efficiencies for reconstructing $\tau^- \to \pi^-\pi^+\pi^-\nu_\tau$, $\tau^- \to K^-\pi^+\pi^-\nu_\tau$, $\tau^- \to K^-K^+\pi^-\nu_\tau$, and $\tau^- \to K^-K^+K^-\nu_\tau$ decays as $\tau^- \to h^-h^+h^-\nu_\tau$ are 26.7%, 27.5%, 27.2%, and 24.8%, respectively, while the reconstruction efficiencies of the dominant background modes, $\tau^- \to \pi^-\pi^+\pi^-\pi^0\nu_\tau$, $\tau^- \to K^0_S\pi^-\nu_\tau$, and $e^+e^- \to q\bar{q}$, are

6.0%, 1.8%, and 0.004%, respectively. The fractions of $\tau^- \to \pi^-\pi^+\pi^-\pi^0\nu_\tau$, $\tau^- \to K^0_S\pi^-\nu_\tau$, $e^+e^- \to q\bar{q}$ and two-photon backgrounds that are reconstructed as $\tau^- \to h^-h^+h^-\nu_\tau$ are 6.47%, 0.34%, 0.35% and 0.05%, respectively; the two-photon background contribution is negligible.

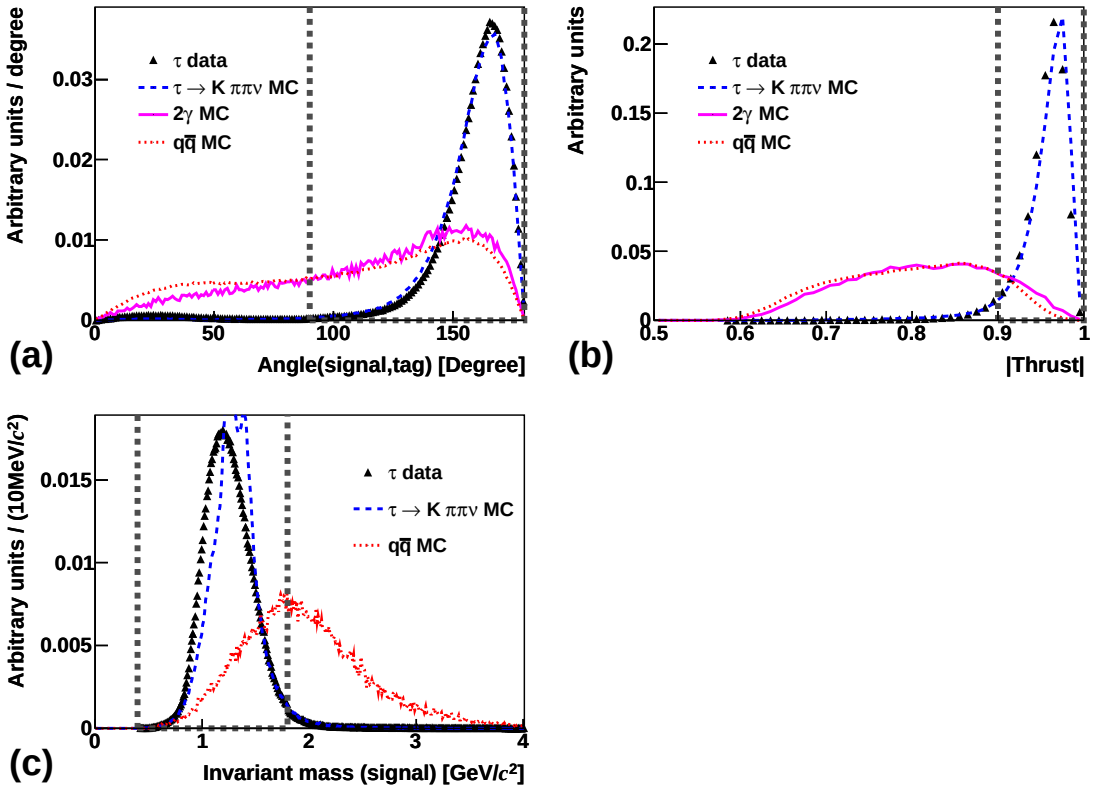


FIG. 2: Distributions of variables used in the event selection. (a) The angle between the total momentum of the hadronic system on the signal-side and the lepton momentum on the tag-side in the CM system. (b) The magnitude of the thrust. (c) The invariant mass of the hadronic system. The triangular points show data, the dashed histograms show the $\tau^- \to K^-\pi^+\pi^-\nu_\tau$ signal MC, the solid histograms show the two-photon background, and the dotted histograms show the $e^+e^- \to q\bar{q}$ background. The dotted vertical lines show the boundaries used to select the signal candidates. All samples are normalized to the same number of events.

An important issue for this analysis is the separation of kaons and pions. In Belle, $dE/dx$ information from the CDC, hit information from the ACC, and time-of-flight measurements from the TOF system are used to construct a likelihood for the kaon (pion) hypothesis, $L(K)$ ($L(\pi)$). Figure 3 shows the kaon likelihood ratio, $L(K)/(L(K)+L(\pi))$, as a function

of momenta. Clean kaon-pion separation is evident over the entire momentum range relevant for this analysis, where the track momentum ranges from 0.1 GeV/$c$ to ∼5 GeV/$c$, and the average momentum is ∼1.3 GeV/$c$. As discussed below, we choose a relatively stringent particle identification (PID) requirement for kaons ($L(K)/(L(K)+L(\pi)) > 0.9$) and a less restrictive one for pions ($L(K)/(L(K)+L(\pi)) < 0.9$). The kaon identification selection has an efficiency of ∼73% for kaons and rejects ∼95% of pions. The kaon and pion identification efficiencies are calibrated using kaon and pion tracks in data from kinematically identified $D^{*+}$ decays, $D^{*+} \to D^0(\to K^-\pi^+)\pi^+$. We evaluate the efficiencies and fake rates for this calibration sample and compare them to Monte Carlo (MC) expectations. From this comparison, we obtain a correction table as a function of track momenta ($p_{lab}$) and polar angles ($\theta_{lab}$), and apply it to the MC. The accuracy of the correction factor, which is the source of the systematic uncertainty of the evaluation of the branching fraction and the mass spectra, is limited by the statistical uncertainties of kaon and pion samples from $D^{*+}$ decays in the certain $p_{lab}$ and $\theta_{lab}$ bins, and the uncertainty of the $D^{*+}$ signal extraction.

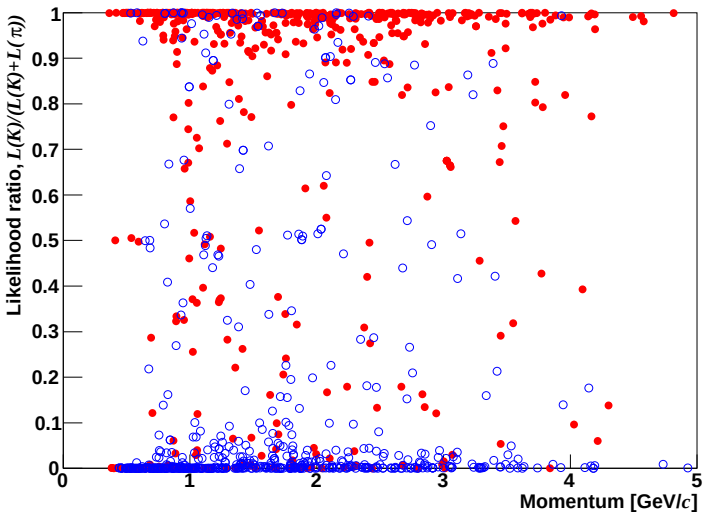


FIG. 3: Likelihood ratio for kaon identification, $L(K)/(L(K)+L(\pi))$, versus particle momentum. The filled and open circles correspond to kinematically identified kaons and pions, respectively.

The kaon identification criterion is determined by maximizing a figure-of-merit (FOM), where the requirement on the kaon identification likelihood ratio is varied. The figure-of-

merit we used is defined as:

$$FOM = \frac{S}{\sqrt{S+N}} \ , \tag{1}$$

where $S$ is the number of signal events and $N$ is the number of cross-feed background events. For the $\tau^- \to K^-\pi^+\pi^-\nu_\tau$ signal ($S$), the cross-feed background component ($N$) includes contributions from $\tau^- \to \pi^-\pi^+\pi^-\nu_\tau$ and $\tau^- \to K^-K^+\pi^-\nu_\tau$ decays. The result of FOM optimization for the $\tau^- \to K^-\pi^+\pi^-\nu_\tau$ decay is shown in Fig. 4, where one can see that FOM is indeed maximal for the particle identification criteria used in this analysis. The same FOM analysis was performed for the $\tau^- \to \pi^-\pi^+\pi^-\nu_\tau$ and $\tau^- \to K^-K^+\pi^-\nu_\tau$ decay modes and resulted in similar particle identification criteria. For electron identification, the likelihood variable is calculated based on the track extrapolation to the ECL, the ratio of the energy deposited in the ECL to the momentum measured in the CDC, the measured $dE/dx$ in the CDC, the shower shape in the ECL, and light yield in the ACC [16]. The extrapolation of tracks from the CDC and SVD to the KLM is used to construct the likelihood variable for muon identification [17]. The efficiencies and systematic uncertainties for lepton identification are evaluated by using a $\gamma\gamma \to e^+e^-/\mu^+\mu^-$ control sample.

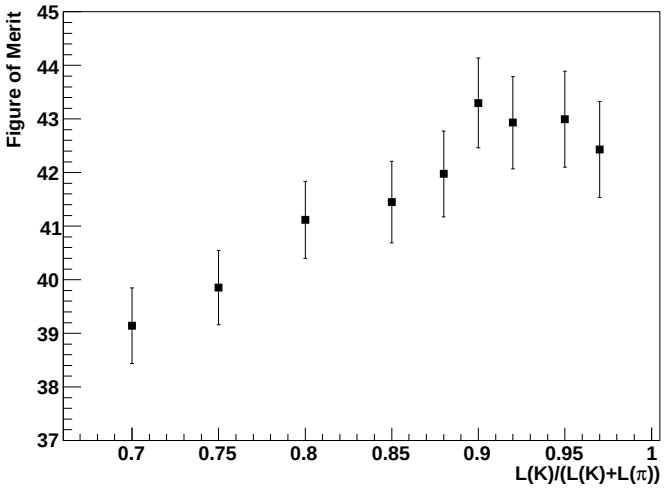


FIG. 4: Figure-of-merit as a function of the likelihood ratio $L(K)/(L(K)+L(\pi))$ requirement, used to separate the kaon and pion hypotheses. The uncertainties are evaluated from the comparison of the efficiencies and fake rates of kaon identification with those of the $D^{*+} \to D^0(\to K^-\pi^+)\pi^+$ control sample.

To reduce the feed-down background and to estimate the remaining backgrounds that

contain $K^0_S$ and $\pi^0$ mesons, we reconstruct $K^0_S$ and $\pi^0$ signals explicitly. $K^0_S$ candidates are formed from oppositely charged pairs of pion tracks with invariant mass $M(\pi\pi)$ within $\pm 13.5$ MeV/$c^2$ ($\pm 5\sigma$) of the $K^0_S$ mass. To improve the $K^0_S$ purity, the point of closest approach to the interaction point along the extrapolation of each track is required to be larger than 0.3 cm in the plane transverse to the beam direction. The azimuthal angle between the momentum vector and the decay vertex vector of the reconstructed $K^0_S$ is required to be less than 0.1 rad. The distance between the two daughter pion tracks at their point of closest approach is required to be less than 1.8 cm, and the flight length of the $K^0_S$ in the plane perpendicular to the beam direction is required to be larger than 0.08 cm. Finally, we require the invariant mass of each $K^0_S$ candidate to be inconsistent with that of a $\Lambda$, $\bar{\Lambda}$, and a photon conversion, where the daughter tracks are assumed to be pions and protons (antiprotons) or electrons and positrons as appropriate. Candidate $\pi^0$'s are reconstructed from pairs of photon clusters. The energy of each photon is required to exceed 50 MeV for candidates in the barrel part of the calorimeter, and 100 MeV for candidates in the endcap part of the calorimeter. We also require the invariant mass of the two photons, $M(\gamma\gamma)$, to be within $\pm$ 16 MeV/$c^2$ of the $\pi^0$ mass. Events containing one or more reconstructed $K^0_S$ or $\pi^0$ are rejected. In addition, in order to reject events containing $\pi^0$'s, we require that there be no photon with energy larger than 0.3 GeV.

## EFFICIENCY ESTIMATION

To estimate the signal efficiency, 97 million signal MC events for the $\tau^- \to \pi^-\pi^+\pi^-\nu_\tau$ decay mode and 5 million signal MC events for each of the $\tau^- \to K^-\pi^+\pi^-\nu_\tau$, $\tau^- \to K^-K^+\pi^-\nu_\tau$, and $\tau^- \to K^-K^+K^-\nu_\tau$ modes were generated using the TAUOLA [18] based KKMC [19] generator. The detector response for all MC data sets was simulated with the GEANT3 [20] package. The TAUOLA generator provides models for $\tau^- \to \pi^-\pi^+\pi^-\nu_\tau$, $\tau^- \to K^-\pi^+\pi^-\nu_\tau$, and $\tau^- \to K^-K^+\pi^-\nu_\tau$ decays, where various intermediate resonances are taken into account. To check whether there is efficiency bias related to the specific decay model used, events with phase-space decay distributions were generated using the KKMC program. The efficiencies as functions of the invariant mass for both $\tau^- \to K^-\pi^+\pi^-\nu_\tau$ decay models are compared in Fig. 5. The relative difference in efficiency between the TAUOLA and phase-space decay models is around 1%. Similarly, very small discrepancies between

the TAUOLA and phase-space decay model are observed in the $\tau^- \to \pi^-\pi^+\pi^-\nu_\tau$ and $\tau^- \to K^-K^+\pi^-\nu_\tau$ decays. We used the TAUOLA decay model to evaluate the efficiencies and their dependencies on the invariant mass of $\tau^- \to \pi^-\pi^+\pi^-\nu_\tau$, $\tau^- \to K^-\pi^+\pi^-\nu_\tau$, and $\tau^- \to K^-K^+\pi^-\nu_\tau$ decays. For the $\tau^- \to K^-K^+K^-\nu_\tau$ decay mode, the TAUOLA generator does not provide any decay model, therefore the efficiency is calculated assuming a phase-space decay. In practice, the efficiencies are evaluated using a two step procedure. First, we evaluate the response matrix for unfolding the mass spectra using the TAUOLA decay model. Next, we recalibrate the efficiencies using the unfolded spectra. Details of this procedure are described in the next section.

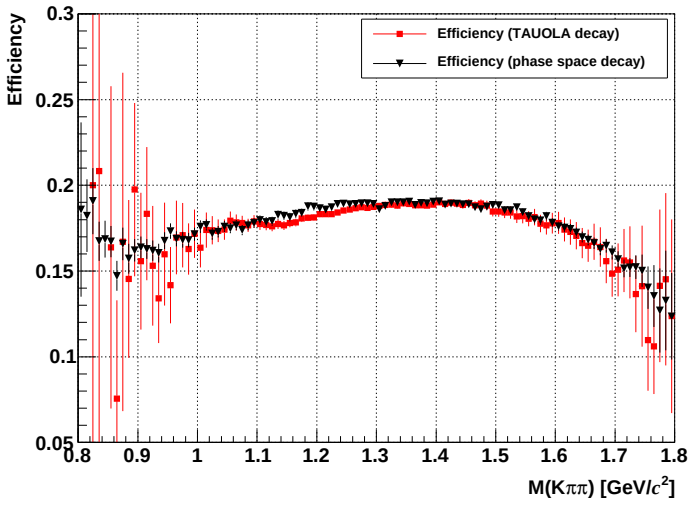


FIG. 5: The efficiency for the $\tau^- \to K^-\pi^+\pi^-\nu_\tau$ decay as a function of $M(K\pi\pi)$. Squares and triangular points represent the TAUOLA decay model and phase-space decay, respectively.

The average efficiencies and the fractions of the cross-feed backgrounds for all three-prong decays are summarized in Table I. The probability of reconstructing $\tau^- \to \pi^-\pi^+\pi^-\nu_\tau$ as $\tau^- \to K^-\pi^+\pi^-\nu_\tau$ is relatively low, but due to the large branching fraction of $\tau^- \to \pi^-\pi^+\pi^-\nu_\tau$ decay, there is a substantial contamination of misidentified $\tau^- \to \pi^-\pi^+\pi^-\nu_\tau$ events in the $\tau^- \to K^-\pi^+\pi^-\nu_\tau$ sample. For a similar reason, the $\tau^- \to K^-K^+K^-\nu_\tau$ decay mode has a large cross-feed background from $\tau^- \to K^-K^+\pi^-\nu_\tau$.

## BRANCHING FRACTION AND MASS SPECTRUM CALCULATION

The numbers of candidate events in the $\tau^- \to \pi^-\pi^+\pi^-\nu_\tau$, $\tau^- \to K^-\pi^+\pi^-\nu_\tau$, $\tau^- \to K^-K^+\pi^-\nu_\tau$, and $\tau^- \to K^-K^+K^-\nu_\tau$ modes, after applying all selection criteria, are summarized in Table II. Possible backgrounds in these signal candidate samples include (a) cross-feed from the signal modes and (b) other processes such as $\tau^- \to \pi^-\pi^+\pi^-\pi^0\nu_\tau$, $\tau^- \to K^0_S\pi^-\nu_\tau$, as well as continuum $e^+e^- \to q\bar{q}$. The fractions of backgrounds coming from other processes are 5% to 12%, as summarized in Table II (fourth column) for each signal mode. The fifth column shows the fraction of the main background component as determined from MC. The mode $\tau^- \to \pi^-\pi^+\pi^-\pi^0\nu_\tau$ dominates for the $\tau^- \to \pi^-\pi^+\pi^-\nu_\tau$ and $\tau^- \to K^-\pi^+\pi^-\nu_\tau$ modes, while the background from continuum $e^+e^- \to q\bar{q}$ is dominant for the $\tau^- \to K^-K^+\pi^-\nu_\tau$ and $\tau^- \to K^-K^+K^-\nu_\tau$ modes.

To take into account the cross-feed between the decay channels, the true yield $N_i^{\rm true}$ ($i$ is the mode number and the values from 1 to 4 correspond to $\tau^- \to \pi^-\pi^+\pi^-\nu_\tau$, $\tau^- \to K^-\pi^+\pi^-\nu_\tau$, $\tau^- \to K^-K^+\pi^-\nu_\tau$, and $\tau^- \to K^-K^+K^-\nu_\tau$), is obtained using the following equation:

$$N_i^{\rm true} = \sum_j (\mathcal{E}^{-1})_{ij}(N_j^{\rm rec} - N_j^{\rm other}) \ , \tag{2}$$

TABLE I: Summary of the efficiencies and the fractions of cross-feed backgrounds. The values in parentheses are the differences of the efficiencies or fake rates from those evaluated directly from the MC with the TAUOLA decay model, $(\mathcal{E}_{ij}^{(2)} - \mathcal{E}_{ij}^{(1)})/\mathcal{E}_{ij}^{(1)}$ in percent (see text).

| | Generated decay mode | | | |
|---|---|---|---|---|
| Reconstructed decay mode | $\tau^- \to \pi^-\pi^+\pi^-\nu_\tau$ | $\tau^- \to K^-\pi^+\pi^-\nu_\tau$ | $\tau^- \to K^-K^+\pi^-\nu_\tau$ | $\tau^- \to K^-K^+K^-\nu_\tau$ |
| $\tau^- \to \pi^-\pi^+\pi^-\nu_\tau$ | 0.22 (−0.1%) | 0.079 (−0.1%) | 0.022 (−1.1%) | $6.4 \times 10^{-3}$ (+2.6%) |
| $\tau^- \to K^-\pi^+\pi^-\nu_\tau$ | 0.012 (−0.2%) | 0.18 (−0.5%) | 0.047 (+1.4%) | 0.019 (−3.1%) |
| $\tau^- \to K^-K^+\pi^-\nu_\tau$ | $3.9 \times 10^{-4}$ (−0.3%) | $4.7 \times 10^{-3}$ (−4.4%) | 0.12 (−1.0%) | 0.051 (−0.4%) |
| $\tau^- \to K^-K^+K^-\nu_\tau$ | $5.0 \times 10^{-6}$ (+4.5%) | $1.3 \times 10^{-4}$ (−9.1%) | $2.3 \times 10^{-3}$ (−14.0%) | 0.081 (+1.2%) |

TABLE II: The number of reconstructed events (second column), the number of true events (third column), the number of background events other than three-prong cross-feeds (fourth column), and the main source of other backgrounds with its fraction of the total (fifth column).

| Decay mode | $N^{\rm rec}$ | $N^{\rm true}$ | $N^{\rm other}$ | Main component in $N^{\rm other}$ |
|---|---|---|---|---|
| $\tau^- \to \pi^-\pi^+\pi^-\nu_\tau$ | $8.86 \times 10^6$ | $3.52 \times 10^7$ | $9.35 \times 10^5$ (10.6%) | $\tau^- \to \pi^-\pi^+\pi^-\pi^0\nu_\tau$ (64.2%) |
| $\tau^- \to K^-\pi^+\pi^-\nu_\tau$ | $7.94 \times 10^5$ | $1.38 \times 10^6$ | $9.60 \times 10^4$ (12.1%) | $\tau^- \to \pi^-\pi^+\pi^-\pi^0\nu_\tau$ (34.4%) |
| $\tau^- \to K^-K^+\pi^-\nu_\tau$ | $1.08 \times 10^5$ | $6.47 \times 10^5$ | $7.16 \times 10^3$ (6.66%) | $e^+e^- \to q\bar{q}$ (30.3%) |
| $\tau^- \to K^-K^+K^-\nu_\tau$ | $3.16 \times 10^3$ | $1.37 \times 10^4$ | $1.71 \times 10^2$ (5.41%) | $e^+e^- \to q\bar{q}$ (53.0%) |

where $N_j^{\rm rec}$ is the number of events for the $j$-th reconstructed decay mode and $N_j^{\rm other}$ is the number of background events in the $j$-th mode. Here $\mathcal{E}_{ij}$ is the efficiency for detecting the $j$-th mode as the $i$-th one. The values of $N^{\rm rec}$ and $N^{\rm other}$ are listed in the second and third columns of Table II, respectively.

We have determined the efficiency (migration) matrix iteratively. First, it is determined using the mass spectra as modeled in the current TAUOLA MC program. (We refer to this efficiency matrix as $\mathcal{E}_{ij}^{(1)}$). As is discussed in the next paragraph, we then unfolded the mass spectra of each mode to obtain the true mass distribution. The resultant unfolded mass spectra are then used to determine the efficiency matrix $\mathcal{E}_{ij}^{(2)}$ using a weighting procedure. The matrix elements $\mathcal{E}_{ij}^{(2)}$ are given in Table I, where the values given in parentheses are the percentage differences between $\mathcal{E}_{ij}^{(1)}$ and $\mathcal{E}_{ij}^{(2)}$; $(\mathcal{E}_{ij}^{(2)} - \mathcal{E}_{ij}^{(1)})/\mathcal{E}_{ij}^{(1)}$. Since the efficiency is smooth as a function of hadronic mass, the difference between $\mathcal{E}_{ij}^{(1)}$ and $\mathcal{E}_{ij}^{(2)}$ is very small ($\sim$1%) in most cases, except for the off-diagonal entries related to the $\tau^- \to K^-K^+K^-\nu_\tau$ mode. The source of these large discrepancies is the mass dependence of the fake rates, together with the considerable differences between the unfolded spectrum and the generated spectrum.

The unfolding procedure extracts the true mass spectra for all four modes, denoted by the vector $\boldsymbol{x}$, by solving the matrix equation $\hat{A}\boldsymbol{x} = \boldsymbol{b}$. In this equation, $\boldsymbol{b}$ is the vector of the reconstructed mass spectrum with backgrounds other than the three-prong cross-feed subtracted, and $\hat{A}$ is the response matrix.

The matrix $\hat{A}$ takes into account the cross-feed between different modes caused by particle misidentification, as well as the effects of finite resolution and the limited acceptance of the detector. The response matrix is obtained by merging 16 sub-response matrices as shown in

Fig. 6. The matrix is determined using the TAUOLA decay model MC simulation. Clear correlations between the measured and generated values are seen along the diagonal parts of $\hat{A}$.

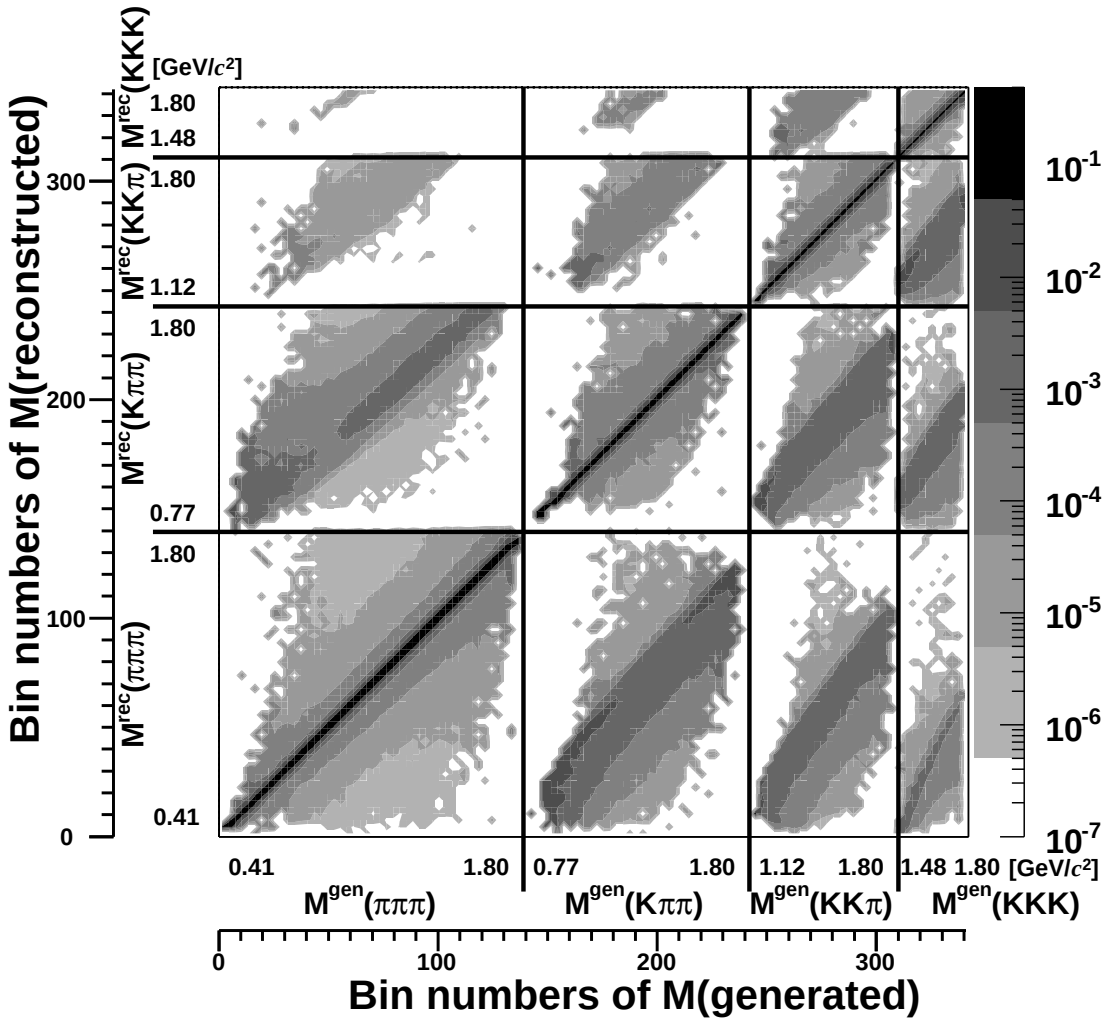


FIG. 6: Response matrix $\hat{A}$ obtained by merging 16 sub-response matrices that represent the efficiency or fake rates among the four three-prong modes. The bin numbers correspond to the following ranges of the invariant masses: (1) from 0 to 138 , 0.41 GeV/$c^2$ to 1.8 GeV/$c^2$ of $M(\pi\pi\pi)$; (2) from 139 to 241 , 0.77 GeV/$c^2$ to 1.8 GeV/$c^2$ of $M(K\pi\pi)$; (3) from 242 to 309 , 1.12 GeV/$c^2$ to 1.8 GeV/$c^2$ of $M(KK\pi)$; and (4) from 310 to 341 , 1.48 GeV/$c^2$ to 1.8 GeV/$c^2$ of $M(KKK)$. All bin sizes are 10 MeV/$c^2$.

For the unfolding algorithm, we follow the method of the ALEPH Collaboration, which is based on the Singular Value Decomposition technique for matrix inversion [21] and advanced

regularization [22]. Two independent $\tau^- \to h^- h^+ h^- \nu_\tau$ signal MC samples are used to check the validity of the unfolding procedure. One sample is used for the determination of the response matrix. We check the reproducibility of the generated $M(hhh)$ mass spectra with the other sample, and find, for the whole mass range, that the differences are less than 1%. These discrepancies are included in the systematic uncertainties of unfolding (UNF1 below). The resulting unfolded normalized mass spectra of the three-prong decays are shown in Fig. 7, where the error bars indicate the statistical uncertainty only, and the gray bands correspond to the systematic uncertainty. Note that the uncertainties common for all bins are taken into account as the systematic uncertainties on the branching fraction (Table IV), while the bin-by-bin errors remained in the normalized mass spectra $1/N(dN/dM)$ are accounted here. The following sources of systematic uncertainties in the mass spectra are considered: the unfolding procedure (UNF1 and UNF2), the kaon identification efficiency (KID), the background estimation other than the three-prong cross-feed (BGE), the effect of $\gamma$ veto (GAM), and the track momentum scale (MOM). Table III summarizes various contributions to the systematic uncertainties on the normalized mass spectra $1/N(dN/dM)$ for each decay mode.

The systematic uncertainty due to the unfolding procedure is determined from MC by comparing the generated and unfolded mass spectra (UNF1). Another estimation of the uncertainty of the unfolding procedure is obtained by changing the value of unfolding parameter that determines the effective rank of the response matrix (UNF2). This is the most important systematic uncertainty for $KKK$ mode. The kaon identification efficiency and the fake rate are calibrated by using $D^{*+}$ sample as described in the previous section. The uncertainties due to the particle identification (KID) are evaluated by varying efficiency and cross-feed fraction by one standard deviation in the response matrix. The systematic uncertainty from the background estimation (BGE) is evaluated by varying the branching fraction values used in the MC by one standard deviation. The uncertainty due to the $\gamma$ veto (GAM) is evaluated by using different selection criteria for photon energy and comparing the resultant unfolded spectra. For the uncertainty from the track momentum scale (MOM), we reconstruct $\phi \to K^+ K^-$ and $D^\pm \to K^\mp \pi^\pm \pi^\pm$ decays. By comparing the reconstructed masses of $\phi$ and $D^\pm$ mesons with their world average values, we conservatively assign 0.01% uncertainty for the momentum scale. By applying this variation to the reconstructed mass spectra of $\tau^- \to h^- h^+ h^- \nu_\tau$ decay and unfolding it, we obtain the uncertainties due to the

momentum scale.

The systematic uncertainty varies as a function of the mass of the hadronic system in each mode. The typical uncertainties averaged over all mass bins are evaluated by summing the systematic uncertainties of each bin and ignoring the correlations between bins, and the results are 0.7%, 2.2%, 2.2%, and 9.5%, for the $\tau^- \to \pi^-\pi^+\pi^-\nu_\tau$, $\tau^- \to K^-\pi^+\pi^-\nu_\tau$, $\tau^- \to K^-K^+\pi^-\nu_\tau$, and $\tau^- \to K^-K^+K^-\nu_\tau$ decay modes, respectively. In practice, we have obtained the covariance matrix for each source of the systematic uncertainties and added them to obtain the total uncertainty. The gray bands in Fig. 7 show the square roots of the diagonal components of the covariance matrix. The off-diagonal components of the covariance matrix are shown in Fig. 8 in term of the correlation coefficients $\rho^{\rm Spec}(i,j)$ defined by $\rho^{\rm Spec}(i,j) = {\rm cov}(i,j)/\sqrt{{\rm cov}(i,i)\cdot{\rm cov}(j,j)}$, where $i$ and $j$ are bin numbers.

Figure 7 shows rather large discrepancies between the mass spectra of the generator and our unfolded spectra except for $\tau^- \to \pi^-\pi^+\pi^-\nu_\tau$ decay. For example, for the $\tau^- \to K^-\pi^+\pi^-\nu_\tau$ mass spectrum (Fig. 7b), it is evident that there are contributions from two resonant peaks, similar to the MC expectations. However, the faster rise of the real data as compared with the MC in the $1.0 - 1.1$ GeV mass region and the fall-off at high masses in the $\tau^- \to K^-\pi^+\pi^-\nu_\tau$ mass spectrum may also be suggestive of a substantial non-resonant component that is not included in the current MC model. The use of the unfolded invariant mass distributions in estimating the efficiencies allows one to compensate for model deficiencies when evaluating the branching fractions.

In order to determine the branching fraction, we normalize to the number of pure leptonic decays, where one $\tau$ decays to $\tau \to e\overline{\nu}\nu$ and the other decays to $\tau \to \mu\overline{\nu}\nu$ [23] (hereafter such events are referred to as $\{\, e, \mu \,\}$ events). The branching fraction for the $i$-th decay mode can then be written as:

$$\mathcal{B}_i = N_i^{\rm true} \cdot \frac{\varepsilon_{e\mu}}{N_{{\rm sig},e\mu}} \cdot \frac{\mathcal{B}_{\tau\to e\overline{\nu}\nu}\cdot\mathcal{B}_{\tau\to\mu\overline{\nu}\nu}}{\mathcal{B}_{\tau\to l\overline{\nu}\nu}} \ , \tag{3}$$

where $N_{{\rm sig},e\mu} = 8.1\times10^6$ and $\varepsilon_{e\mu} = 0.221 \pm 0.003$ are the number of $\{\, e, \mu \,\}$ events and the corresponding detection efficiency, respectively. The uncertainty in $\varepsilon_{e\mu}$ is determined from the lepton identification uncertainties. Here $\mathcal{B}_{\tau\to e\overline{\nu}\nu} = 0.178$ and $\mathcal{B}_{\tau\to\mu\overline{\nu}\nu} = 0.174$ are the branching fractions of $\tau \to e\overline{\nu}\nu$ and $\tau \to \mu\overline{\nu}\nu$ decays, respectively, and $\mathcal{B}_{\tau\to l\overline{\nu}\nu} =$

TABLE III: Summary of the relative errors of the unfolded mass spectra, $1/N(dN/dM)$ (in %) from different sources of uncertainties: the unfolding procedure (UNF1, UNF2), the kaon identification (KID), the background estimation (BGE), the $\gamma$ veto (GAM), and the momentum scale (MOM). The "average" uncertainties (the 2nd, 4-th, 6-th, and 8-th columns) are evaluated by taking average of errors in all bins. The "peak" uncertainties (the 3rd, 5-th, 7-th, and 9-th columns) represent the errors at the peak position of the spectra. See the text for a more detailed description.

| Sources of | $\tau \to \pi\pi\pi\nu$ | | $\tau \to K\pi\pi\nu$ | | $\tau \to KK\pi\nu$ | | $\tau \to KKK\nu$ | |
|---|---|---|---|---|---|---|---|---|
| uncertainties | average | peak | average | peak | average | peak | average | peak |
| (UNF1) | 0.5 | 0.5 | 0.1 | 0.1 | 0.4 | 0.4 | 0.6 | 0.6 |
| (UNF2) | 0.1 | 0.1 | 1.6 | 1.5 | 0.9 | 0.9 | 7.3 | 4.0 |
| (KID) | 0.4 | 0.4 | 1.0 | 0.8 | 1.5 | 1.1 | 1.9 | 0.9 |
| (BGE) | 0.2 | 0.2 | 0.6 | 0.5 | 0.4 | 0.3 | 1.9 | 1.1 |
| (GAM) | 0.6 | 0.4 | 0.9 | 0.4 | 1.2 | 0.9 | 4.6 | 3.2 |
| (MOM) | 0.1 | 0.0 | 0.4 | 0.2 | 0.3 | 0.3 | 2.7 | 3.1 |
| Total systematics | 0.7 | 0.7 | 2.2 | 1.9 | 2.2 | 1.7 | 9.5 | 6.2 |
| Statistics | 0.2 | 0.2 | 1.1 | 0.8 | 1.0 | 0.8 | 7.1 | 4.6 |
| Total | 0.9 | 0.8 | 2.4 | 2.0 | 2.4 | 1.9 | 11.8 | 7.7 |

$\mathcal{B}_{\tau\to e\overline{\nu}\nu} + \mathcal{B}_{\tau\to\mu\overline{\nu}\nu}$. The true yields $N_i^{\rm true}$ obtained from Eq. 2 are given in the third column of Table II.

This normalization method requires a precise measurement of the number of $\{ e, \mu \}$ events and a careful determination of the corresponding efficiency. Figure 9 shows a comparison of the invariant mass of the electron and muon system and the cosine of the angle between electron and muon, for real $\{ e, \mu \}$ events and the sum of MC expectations. The MC reproduces the data reasonably well. The background fraction is estimated to be 5.9% using MC. After subtracting background, we obtain the number of $\{ e, \mu \}$ events.

Figure 10 shows the observed distributions of $M(\pi\pi\pi)$, $M(K\pi\pi)$, $M(KK\pi)$, and $M(KKK)$. The backgrounds are represented by the hatched and the gray histograms for the

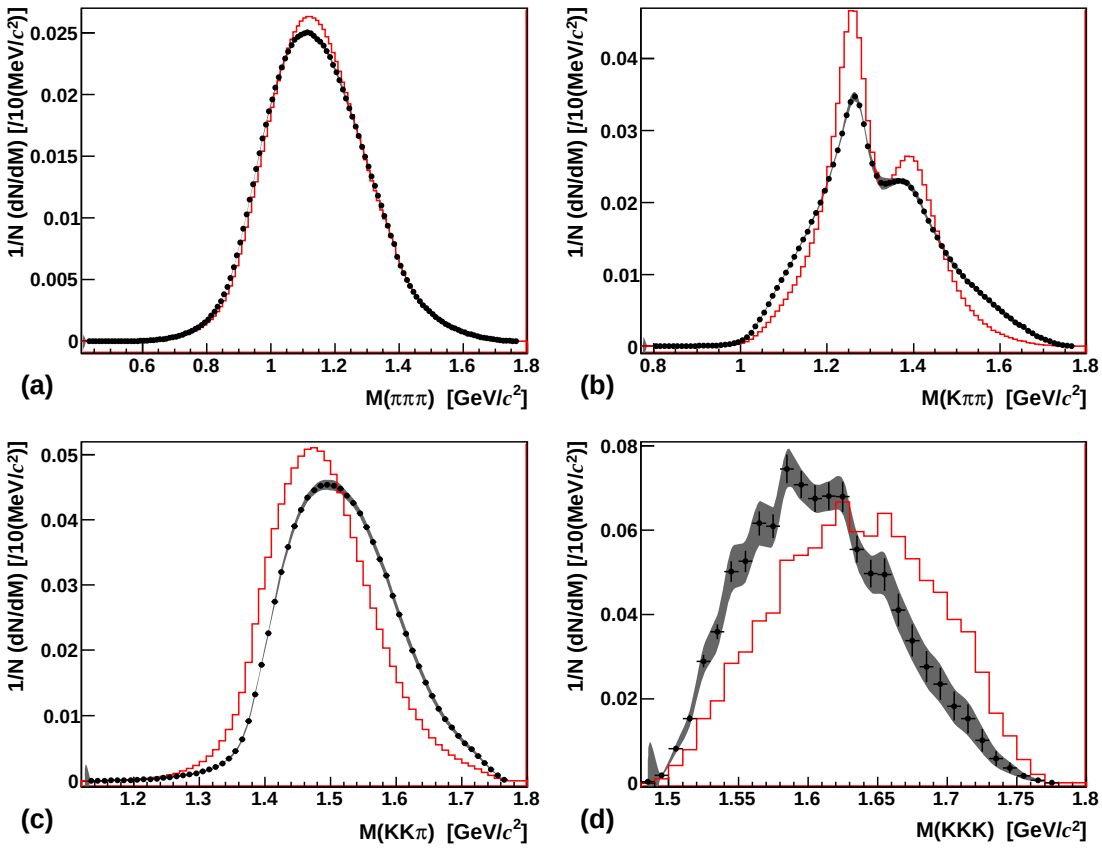


FIG. 7: The unfolded mass spectra of the three-prong decays, $1/N(dN/dM)$: (a) $M(\pi\pi\pi)$ distribution of $\tau^- \to \pi^-\pi^+\pi^-\nu_\tau$, (b) $M(K\pi\pi)$ distribution of $\tau^- \to K^-\pi^+\pi^-\nu_\tau$, (c) $M(KK\pi)$ distribution of $\tau^- \to K^-K^+\pi^-\nu_\tau$, and (d) $M(KKK)$ distribution of $\tau^- \to K^-K^+K^-\nu_\tau$. The black points correspond to the unfolded mass spectra with statistical uncertainties only, and the gray bands correspond to the systematic uncertainty. The solid histograms are the model predictions implemented in the current TAUOLA MC simulation.

sum of the three-prong cross-feed backgrounds and other background components, respectively. Note that the three-prong cross-feed backgrounds are determined by the unfolding procedure previously described.

Table IV summarizes various contributions to the systematic uncertainties on the branching fractions. The uncertainty in the track-finding efficiency is estimated from a comparison of real and MC data for the $D^* \to \pi D^0$, $D^0 \to \pi\pi K^0_S(K^0_S \to \pi^+\pi^-)$ decay sample. The uncertainties due to the kaon and pion identification are evaluated by applying the uncertainties in kaon identification efficiencies to the efficiency matrix in Table I. First, we

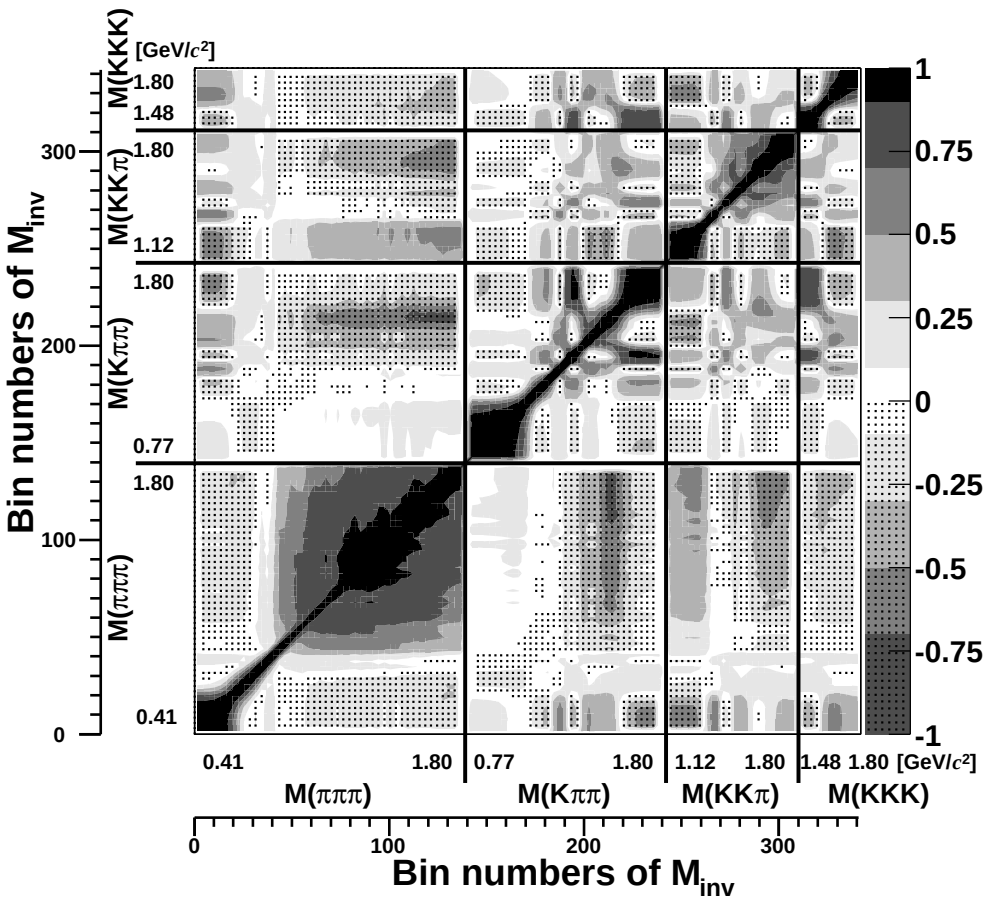


FIG. 8: The correlation coefficients of the unfolded mass spectra for three-prong decays. See Fig. 6 for the convention of the bin numbers. The pattern is the reflection of the detailed unfolding procedure.

measure the kaon and pion identification efficiencies and their uncertainties using the control sample of $D^{*+} \to D^0\pi_s^+$ and $D^0 \to K^-\pi^+$ events. Since these efficiencies are applied to the efficiency matrix, we propagate the uncertainties in the kaon and pion identification efficiencies to the covariance matrix of branching fraction measurement. The kaon identification systematic uncertainties for $\tau^- \to \pi^-\pi^+\pi^-\nu_\tau$, $\tau^- \to K^-\pi^+\pi^-\nu_\tau$, $\tau^- \to K^-K^+\pi^-\nu_\tau$, and $\tau^- \to K^-K^+K^-\nu_\tau$ decays are 1.3%, 3.9%, 1.9%, and 5.4%, respectively. For lepton identification efficiency uncertainties, we use $\gamma\gamma \to e^+e^-/\mu^+\mu^-$ events.

In order to take into account the effects of the mass spectra on the branching fraction measurements, we have determined the mass spectra of the four dominant decay modes iteratively. The uncertainties in branching fractions due to the mass spectra are evaluated

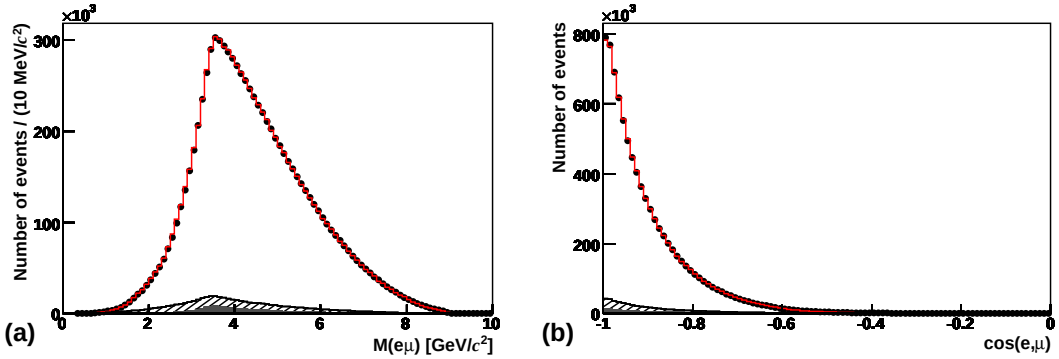


FIG. 9: Distributions of the $\{ e, \mu \}$ events: (a) Invariant mass of the electron–muon system. (b) Cosine of the angle between the electron and muon. The closed circles and the solid histogram represent the data and the sum of the MC expectations, respectively. The open histogram represents the $\{ e, \mu \}$ signal events, while the $\tau$-pair background and the two-photon background are shown by the hatched and the gray histograms, respectively.

by varying the unfolded spectra by one standard deviation of their statistical and systematic errors, assuming 100% bin-by-bin correlations for systematic errors. The trigger efficiency for the three-prong modes is ∼86% with an uncertainty of ∼0.6%. This efficiency is obtained using a trigger simulation program applied to the signal MC samples. The uncertainty due to the $\gamma$ veto is evaluated by using different selection criteria for photon energy. The uncertainty due to the $K^0_S$ veto is evaluated by removing the veto requirement. The uncertainties in background estimation include the effect of luminosity, the cross section for $e^+e^- \to \tau^+\tau^-$, and the subtraction of background from non-three-prong $\tau$ decays and continuum $e^+e^- \to q\bar{q}$. The uncertainty on the $\tau$ decay background subtraction is evaluated by propagating the errors from the $\tau$ branching fractions other than those with three-prongs. The fraction of the $e^+e^- \to q\bar{q}$ background is negligible for $\tau^- \to \pi^-\pi^+\pi^-\nu_\tau$ and $\tau^- \to K^-\pi^+\pi^-\nu_\tau$ modes, and is $2.0 \pm 0.2\%$ and $2.9 \pm 0.3\%$ for $\tau^- \to K^-K^+\pi^-\nu_\tau$ and $\tau^- \to K^-K^+K^-\nu_\tau$ modes, respectively. The uncertainties in the $e^+e^- \to q\bar{q}$ background are estimated from comparison of the number of events in data and $e^+e^- \to q\bar{q}$ MC, in the mass region above the $\tau$ mass. The effects of the uncertainties in the luminosity and the cross section for $e^+e^- \to \tau^+\tau^-$ [24] are negligible because we use $\{ e, \mu \}$ events for normalization. The uncertainties in the leptonic decay branching fractions for the $\tau$ are also taken into account.

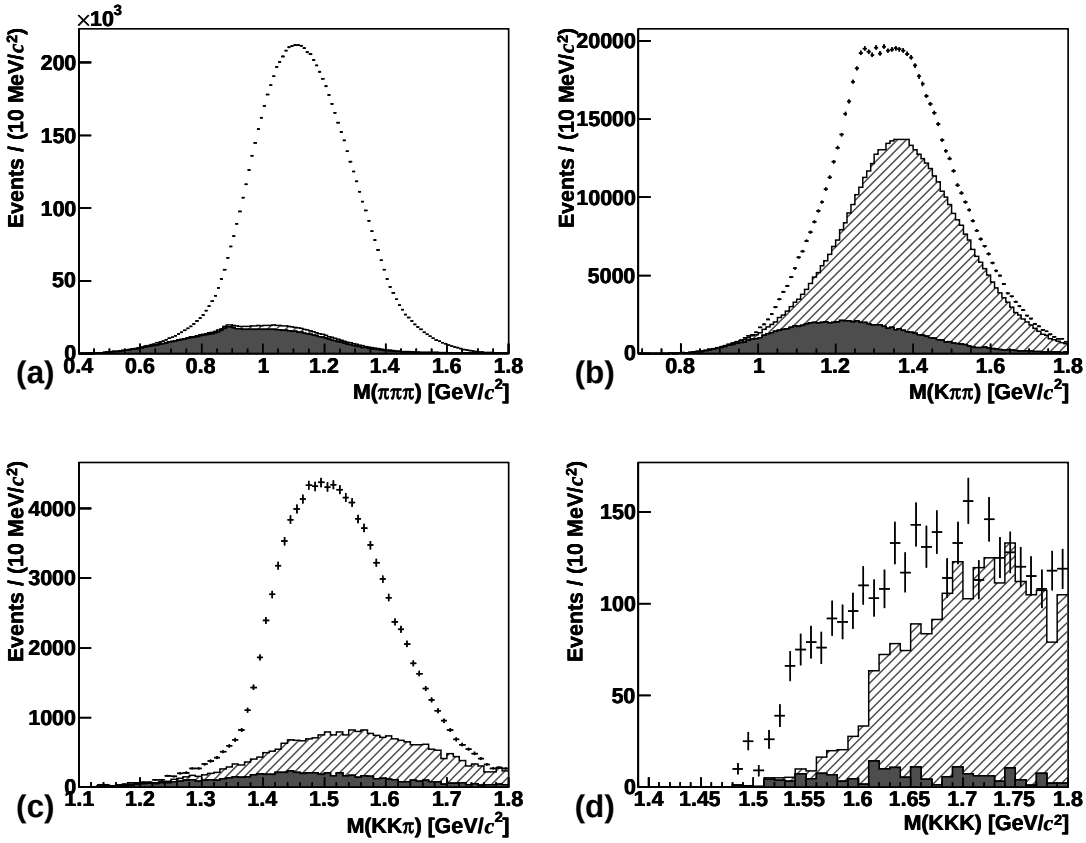


FIG. 10: The reconstructed invariant mass distributions: (a) $M(\pi\pi\pi)$ distribution for $\tau^- \to \pi^-\pi^+\pi^-\nu_\tau$, (b) $M(K\pi\pi)$ distribution for $\tau^- \to K^-\pi^+\pi^-\nu_\tau$, (c) $M(KK\pi)$ distribution for $\tau^- \to K^-K^+\pi^-\nu_\tau$, and (d) $M(KKK)$ distribution for $\tau^- \to K^-K^+K^-\nu_\tau$. For all histograms, the black points with error bars represent the data, the gray histograms are the sum of all backgrounds other than the three-prong cross-feed, and the hatched histograms are the sum of three-prong cross-feed backgrounds. Note that the cross-feed backgrounds are estimated from the unfolding of the data. The uncertainties shown for the data are statistical only.

After taking into account the backgrounds, the efficiencies and various sources of systematic uncertainties discussed above, we obtain the following branching fractions for three-prong decays:

TABLE IV: Summary of the systematic uncertainties on the branching fractions (%).

| Source | $\tau \to \pi\pi\pi\nu$ | $\tau \to K\pi\pi\nu$ | $\tau \to KK\pi\nu$ | $\tau \to KKK\nu$ |
|---|---|---|---|---|
| Tracking efficiency | $+2.2/-2.0$ | $+2.1/-2.0$ | $+2.1/-2.0$ | $+2.1/-1.9$ |
| Particle ID | $\pm1.9$ | $+4.0/-4.1$ | $\pm2.3$ | $+5.4/-5.6$ |
| Mass spectrum | $\pm0.1$ | $\pm0.1$ | $\pm0.1$ | $+0.5/-0.8$ |
| Trigger efficiency | $\pm0.5$ | $\pm0.5$ | $\pm0.6$ | $\pm0.6$ |
| $\gamma$ veto | $\pm0.9$ | $\pm1.5$ | $\pm1.7$ | $\pm0.5$ |
| $K^0_S$ veto | $\pm0.2$ | $\pm0.2$ | $\pm0.1$ | $\pm0.3$ |
| Background estimation | $\pm0.3$ | $\pm1.3$ | $\pm0.3$ | $\pm0.4$ |
| Leptonic branching fraction | $\pm0.2$ | $\pm0.2$ | $\pm0.2$ | $\pm0.2$ |
| Total | $+3.1/-3.0$ | $\pm5.0$ | $\pm3.6$ | $+5.9/-6.0$ |

$$\begin{aligned}
\mathcal{B}(\tau^- \to \pi^-\pi^+\pi^-\nu_\tau) &= (8.42 \pm 0.00(\text{stat.})^{+0.26}_{-0.25}(\text{sys.})) \times 10^{-2} \ ,^{1} \\
\mathcal{B}(\tau^- \to K^-\pi^+\pi^-\nu_\tau) &= (3.30 \pm 0.01(\text{stat.})^{+0.16}_{-0.17}(\text{sys.})) \times 10^{-3} \ , \\
\mathcal{B}(\tau^- \to K^-K^+\pi^-\nu_\tau) &= (1.55 \pm 0.01(\text{stat.})^{+0.06}_{-0.05}(\text{sys.})) \times 10^{-3} \ , \text{ and} \\
\mathcal{B}(\tau^- \to K^-K^+K^-\nu_\tau) &= (3.29 \pm 0.17(\text{stat.})^{+0.19}_{-0.20}(\text{sys.})) \times 10^{-5} \ .
\end{aligned}$$

The covariance matrices for the branching fraction measurements are given in Table V in terms of the correlation coefficients $\rho^{\rm BF}(i,j) = \text{cov}(i,j)/\sqrt{\text{cov}(i,i)\cdot\text{cov}(j,j)}$, where $i$ and $j$ correspond to one of the four three-prong decay modes. There is a strong correlation between $\tau^- \to \pi^-\pi^+\pi^-\nu_\tau$ and $\tau^- \to K^-\pi^+\pi^-\nu_\tau$ decays, which mostly comes from the effect of kaon identification.

Using the results of the branching fractions and the correlation matrix, the ratios of the branching fractions involving kaons to the branching fraction of $\tau^- \to \pi^-\pi^+\pi^-\nu_\tau$ decay are

[1] The actual value of the statistical uncertainty of $\mathcal{B}(\tau^- \to \pi^-\pi^+\pi^-\nu_\tau)$ is $0.003 \times 10^{-2}$.

TABLE V: The correlation coefficients in the branching fraction measurements.

| | $\tau^- \to$ $K^-\pi^+\pi^-\nu_\tau$ | $\tau^- \to$ $K^-K^+\pi^-\nu_\tau$ | $\tau^- \to$ $K^-K^+K^-\nu_\tau$ |
|---|---|---|---|
| $\tau^- \to \pi^-\pi^+\pi^-\nu_\tau$ | $+0.175$ | $+0.049$ | $-0.053$ |
| $\tau^- \to K^-\pi^+\pi^-\nu_\tau$ | | $+0.080$ | $+0.035$ |
| $\tau^- \to K^-K^+\pi^-\nu_\tau$ | | | $-0.008$ |

estimated:

$$\begin{aligned}
\mathcal{B}(\tau^- \to K^-\pi^+\pi^-\nu_\tau)/\mathcal{B}(\tau^- \to \pi^-\pi^+\pi^-\nu_\tau) &= (3.92 \pm 0.02^{+0.15}_{-0.16}) \times 10^{-2} \ , \\
\mathcal{B}(\tau^- \to K^-K^+\pi^-\nu_\tau)/\mathcal{B}(\tau^- \to \pi^-\pi^+\pi^-\nu_\tau) &= (1.84 \pm 0.01 \pm 0.05) \times 10^{-2} \ , \text{ and} \\
\mathcal{B}(\tau^- \to K^-K^+K^-\nu_\tau)/\mathcal{B}(\tau^- \to \pi^-\pi^+\pi^-\nu_\tau) &= (3.90 \pm 0.20^{+0.22}_{-0.23}) \times 10^{-4} \ ,
\end{aligned}$$

where the first and the second uncertainties are statistical and systematic, respectively.

## DISCUSSION

The results of this analysis for the branching fractions of various three-prong modes are listed in Table VI together with recent results from BaBar [7]. Note that for the $\tau^- \to \pi^-\pi^+\pi^-\nu_\tau$ and $\tau^- \to K^-\pi^+\pi^-\nu_\tau$ modes, the branching fractions listed do not include any $K^0$ contribution.

TABLE VI: Comparison of the branching fraction results

| Decay mode | BaBar | Belle |
|---|---|---|
| $\tau^- \to \pi^-\pi^+\pi^-\nu_\tau$, % | $8.83 \pm 0.01 \pm 0.13$ | $8.42 \pm 0.00^{+0.26}_{-0.25}$ |
| $\tau^- \to K^-\pi^+\pi^-\nu_\tau$, % | $0.273 \pm 0.002 \pm 0.009$ | $0.330 \pm 0.001^{+0.016}_{-0.017}$ |
| $\tau^- \to K^-K^+\pi^-\nu_\tau$, % | $0.1346 \pm 0.0010 \pm 0.0036$ | $0.155 \pm 0.001^{+0.006}_{-0.005}$ |
| $\tau^- \to K^-K^+K^-\nu_\tau$, $10^{-5}$ | $1.58 \pm 0.13 \pm 0.12$ | $3.29 \pm 0.17^{+0.19}_{-0.20}$ |

In Fig. 11, our results are compared with the previous measurements. For all modes studied, the precision of the branching fractions for both BaBar and Belle is significantly

higher than before. The accuracy of our results is comparable to that of BaBar, but the central values show striking differences in all channels other than $\tau^- \to \pi^-\pi^+\pi^-\nu_\tau$. For the $\tau^- \to \pi^-\pi^+\pi^-\nu_\tau$ mode, our result is $1.4\sigma$ lower than that of BaBar, while for other modes the branching fractions obtained by Belle are higher by $3.0\sigma$, $3.0\sigma$, and $5.4\sigma$ than those of BaBar for the $\tau^- \to K^-\pi^+\pi^-\nu_\tau$, $\tau^- \to K^-K^+\pi^-\nu_\tau$, and $\tau^- \to K^-K^+K^-\nu_\tau$ modes, respectively.

## CONCLUSION

Using a data sample of $6.12\times10^8$ $\tau^+\tau^-$ pairs collected with the Belle detector, we measure the branching fractions for the $\tau^- \to \pi^-\pi^+\pi^-\nu_\tau$, $\tau^- \to K^-\pi^+\pi^-\nu_\tau$, $\tau^- \to K^-K^+\pi^-\nu_\tau$, and $\tau^- \to K^-K^+K^-\nu_\tau$ decay modes. We have been able to extract unfolded invariant mass spectra for all four modes (Fig. 7) by taking into account the cross-feed effects. A future detailed analysis of these spectra as well as those of the intermediate two-body states will allow studies of the decay dynamics to be performed.

## ACKNOWLEDGMENTS

We thank the KEKB group for the excellent operation of the accelerator, the KEK cryogenics group for the efficient operation of the solenoid, and the KEK computer group and the National Institute of Informatics for valuable computing and SINET3 network support. We acknowledge support from the Ministry of Education, Culture, Sports, Science, and Technology (MEXT) of Japan, the Japan Society for the Promotion of Science (JSPS), and the Tau-Lepton Physics Research Center of Nagoya University; the Australian Research Council and the Australian Department of Industry, Innovation, Science and Research; the National Natural Science Foundation of China under contract No. 10575109, 10775142, 10875115 and 10825524; the Department of Science and Technology of India; the BK21 and WCU program (grant No. R32-2008-000-10155-0) of the Ministry Education Science and Technology, the CHEP SRC program and Basic Research program (grant No. R01-2008-000-10477-0) of the Korea Science and Engineering Foundation, Korea Research Foundation (KRF-2008-313-C00177), and the Korea Institute of Science and Technology Information; the Polish Ministry of Science and Higher Education; the Ministry of Education and Science of the

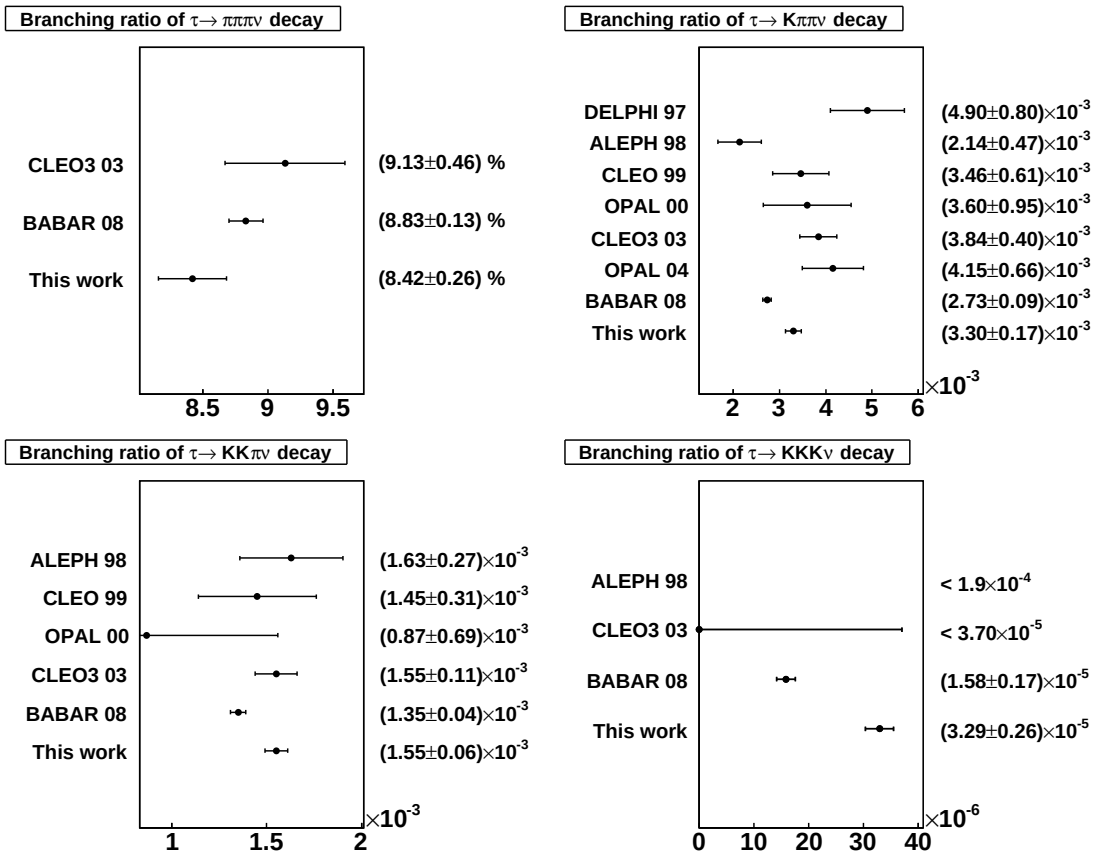


FIG. 11: Summary of the branching fraction measurements of three-prong $\tau$ decays.

Russian Federation and the Russian Federal Agency for Atomic Energy; the Slovenian Research Agency; the Swiss National Science Foundation; the National Science Council and the Ministry of Education of Taiwan; and the U.S. Department of Energy. This work is supported by a Grant-in-Aid from MEXT for Science Research in a Priority Area ("New Development of Flavor Physics"), and from JSPS for Creative Scientific Research ("Evolution of Tau-lepton Physics").

[1] J. Wess and B. Zumino, Phys. Lett. B **37**, 95 (1971); E. Witten, Nucl. Phys. B **223**, 422 (1983); *ibid.* **223**, 433 (1983).

[2] U. Kilian *et al.*, Z. Phys. C **62**, 413 (1994); K. Kiers *et al.* Phys. Rev. D **78**, 113008 (2008).

[3] E. Gámiz *et al.*, Phys. Rev. Lett. **94**, 011803 (2005).

[4] R. Barate *et al.* (ALEPH Collaboration), Eur. Phys. J. C **4**, 29 (1998).

[5] G. Abbiendi *et al.* (OPAL Collaboration), Eur. Phys. J. C **35**, 437 (2004).

[6] R. A. Briere *et al.* (CLEO Collaboration), Phys. Rev. Lett. **90**, 181802 (2003).

[7] B. Aubert *et al.* (BABAR Collaboration), Phys. Rev. Lett. **100**, 011801 (2008).

[8] C. Amsler *et al.* (Particle Data Group), Phys. Lett. B **667**, 1 (2008) and 2009 partial update for the 2010 edition.

[9] R. Barate *et al.* (ALEPH Collaboration), Eur. Phys. J. C **11**, 599 (1999).

[10] G. Abbiendi *et al.* (OPAL Collaboration), Eur. Phys. J. C **13**, 197 (2000).

[11] D. M. Asner *et al.* (CLEO Collaboration), Phys. Rev. D **62**, 072006 (2000).

[12] M. Finkemeier and E. Mirkes, Z. Phys. C **69**, 243 (1996).

[13] S. Kurokawa and E. Kikutani, Nucl. Instr. and. Meth. A **499**, 1 (2003), and other papers included in this volume.

[14] A. Abashian *et al.* (Belle Collaboration), Nucl. Instr. and Meth. A **479**, 117 (2002).

[15] M. Fujikawa, H. Hayashii *et al.* (Belle Collaboration), Phys. Rev. D **78**, 072006 (2008).

[16] K. Hanagaki *et al.*, Nucl. Instr. and Meth. A **485**, 490 (2002).

[17] A. Abashian *et al.*, Nucl. Instr. and Meth. A **491**, 69 (2002).

[18] S. Jadach and Z. Wąs, Comp. Phys. Commun. **85**, 453 (1995); Z. Wąs and P. Golonka, Nucl. Phys. Proc. Suppl. **144**, 88 (2005).

[19] S. Jadach, B.F.L. Ward, and Z. Wąs, Comp. Phys. Commun. **130**, 260 (2000); Phys. Rev. **D63**, 113009 (2001).

[20] R. Brun *et al.*, GEANT 3.21, CERN Report DD/EE/84-1, (1984).

[21] A. Höcker and V. Kartvelishvili, Nucl. Instr. and Meth. A **372**, 469 (1996). The FORTRAN implementation of this algorithm can be found at `http://www.lancs.ac.uk/users/spc/staff/karvelishvili.htm`.

[22] Per Christian Hansen, *Rank-deficient and discrete ill-posed problems : numerical aspects of linear inversion*, SIAM, Philadelphia (1997).

[23] D. Epifanov *et al.* (Belle Collaboration), Phys. Lett. B **654**, 65 (2007).

[24] S. Banerjee, B. Pietrzyk, J. M. Roney and Z. Wąs, Phys. Rev. D **77**, 054012 (2008).